Solvothermal Synthesis of Weakly Crystalline Cobalt-Nickel Sulfide to Obtain High Pseudocapacitance

Nao Zhang
China University of Mining and Technology - Xuzhou Campus: China University of Mining and Technology
Ya-bo Zhu (zhuyabo@163.com)
China University of Mining and Technology https://orcid.org/0000-0002-8195-330X
Tingting Xie
China University of Mining and Technology - Xuzhou Campus: China University of Mining and Technology
Chao Shi
China University of Mining and Technology - Xuzhou Campus: China University of Mining and Technology
Qian Xu
China University of Mining and Technology - Xuzhou Campus: China University of Mining and Technology
Guanglan Wang
China University of Mining and Technology - Xuzhou Campus: China University of Mining and Technology
Peizhong Feng
China University of Mining and Technology - Xuzhou Campus: China University of Mining and Technology

Research Article

Keywords: Nickel Cobalt Sulfide, Synthesis time, Crystallinity, Electrochemical property

Posted Date: February 11th, 2021

DOI: https://doi.org/10.21203/rs.3.rs-184247/v1

Version of Record: A version of this preprint was published at Journal of Materials Science: Materials in Electronics on April 2nd, 2021. See the published version at https://doi.org/10.1007/s10854-021-05769-x.

Abstract

In this paper, a dual solvent system of glycerol and ethylene glycerol was used to prepare nickel cobalt sulfide with different crystallinity. It was found that the crystallinity and morphology of the product had an important effect on its electrochemical performance. Therefore, the synthesis time was chosen between 1 and 18 h to control the crystallinity. The best sample (GENCS-3) was prepared within 3hour, and had flower-like structures. Its electrochemical tests showed that it had good ion transmission efficiency and excellent specific capacitance (1816F/g at 1A/g, 1620F/g at 10 A/g). Especially, its retention rate could arrive at 89.5% after 1000 cycles under a current density of 5A/g. The weak crystalline nickel-cobalt sulfide is easy to form porous structure, which can significantly increase capacitance, also maintaining good rate performance.

1. Introduction

As an important energy storage apparatus, supercapacitor has attracted widespread attention all over the world.[1, 2] Pseudocapacitors are also called electrochemical capacitors, which store charge through a reversible redox reaction that occurs on or near the surface of their electrode material. During the reversible redox, pseudocapacitors can keep storing energy to a high energy density. [3-8] However, their electrodes are a key factor affecting their performances as supercapacitors. People are looking for good electrode materials and hope that these electrodes will not only be highly active, but also environmentally friendly and affordable. In recent years, Cobalt-nickel sulfide has always been a hot spot in the field of electrode materials, and has been highly expected. The material has more than one morphology and its sea urchin-like, flower-like and nano-sheet morphology has also been developed and researched.[9-11] Our team has carried out a series of studies on the material as a capacitive electrode.[12-14] We have successfully prepared a serial of products of Nickel-cobalt compounds with different shapes, which were at last transformed into honeycomb-like cobalt nickel sulfatide through room temperature sulfidation. And the obtained honeycomb nickel cobalt sulfatide showed a high specific capacity (1020 F/g) at large current density (30 A/g), and good cycle stability (82.35% after 3000 cycles).[15] We also used solvothermal method in the preparation of nickel cobalt sulfide. We selected isopropanol and ethylene glycol as the mixed solvent unit and changed their ratio to observe the morphology of the corresponding products. It is interested that some of the obtained samples were also honeycomb structure, showing a capacity of 1244 F/g at 1 A/g after adding rGO.[12] Further, we also used various double-solvent systems, including EG–IPA, glycerol–IPA, EG–methanol and EG–ethanol etc., to fabricate nickel cobalt sulfide. Of course, the choice of different solvents here was to understand the effect of solvent components on the morphology of the products. We did obtain various morphologies of nickel cobalt sulfide, including granular-structure, hollow sphere-structure, honeycomb-structure, irregular sphere-like structure and so on. As expected, the honeycomb structure samples still performed best, with capacity of up to 1464F/g.[14]

Recently, a new study has been made in recent experiments on nickel cobalt sulfide. We found that the weak crystalline samples exhibited better capacitive performance than before. In the experiments,

solvothermal method was used for the preparation and a two-solvent system of glycerol and isopropanol was adopted. The morphology and crystallinity of the products were controlled by reaction time. The results showed that all products are irregular particle with closed cavities. Of course, under short synthesis time, some cavitied were opened, showing flower-like shape. The samples with the flower shape could be not crystallized well, but they could have a capacitance of up to 1800 F/g.

2. Experimental

2.1 Synthesis of Cobalt Nickel Sulfide

All chemicals are purchased from commercial channels with high purity. In typical procedure, first of all, 1.2 mmol $Ni(NO_3)_2$·6H2O, 2.4 mmol $Co(NO_3)_2$·6H2O and 4.3 mmol Hexamethyltetramine (HTM) chemical reagents were added to 60ml mixed solution of glycerol and ethylene glycol with 1:3, stirring for 1h to obtain pink solution. Secondly, 6mmol thioacetamide (TAA) were added dropwise to the above solution, which was then transferred into a 100mL Teflon lined autoclave in a furnace. Subsequently the furnace temperature was raised to 453.15 K, keeping the temperature for different times. After cooling to room temperature naturally, the products were washed, separated and dried. The reaction time was selected as 1h, 3h, 6h, 9h, 12h, 15h and 18h, respectively. The obtained samples were named as GENCS-X, where G, E, NCS and X represent glycerol, ethylene glycol, $NiCo_2S_4$, and reaction time, respectively. These samples and their corresponding preparation time are also listed in Table 1.

Table 1
The samples and their reaction time

sample	GENCS-1	GENCS-3	GENCS-6	GENCS-9	GENCS-12	GENCS-15	GENCS-18
Solvent	15mlG+45ml EG						
Synthesis time (hour)	1	3	6	9	12	15	18
Product	$NiCo_2S_4$						

2.2 Structure and morphology characterization

The means of characterization include X-RAY diffraction (XRD) (D8 ADVANCE of Bruker, Germany), Scanning electron microscope (SEM), transmission electron microscope (TEM), Energy dispersive spectrometer (EDS) (Quanta 250, USA) and BET surface area (ASAP 2020 Plus HD88 surface area porosity analyzer of Micromeritics).

2.3 Electrochemical measurement

Electrochemical properties were tested in three-electrode electrochemical cell. The electrochemical properties of the resulting electrodes were studied by using 6M KOH solution as electrolyte. The work electrode was fabricated from a mixture of 80wt% cobalt-nickel sulphide material, 10wt% acetylene black and 10wt% polyvinylidene difluoride binder. After blending, these mixtures were coated onto a clean nickel foam with an effective geometric area of 1×1 cm^2 and then dried under vacuum for 12 h at 60 °C. The mass load for $NiCo_2S_4$ was calculated to be around 3.0 mg/cm^2. The platinum foil (1.5×1.5 cm^2) and a mercuric oxide electrode was used as the counter and reference electrode, respectively. The cyclic voltammetry (CV), galvanostatic charge-discharge (GCD) and electrochemical impedance spectroscopy (EIS) were tested by CHI660D electrochemical workstation. The cycle stability was tested with LANHE test system under a current density of 5A/g.

3. Results And Discussions

3.1 Crystal structure characterization (XRD)

Fig. 1(a) shows the XRD patterns of all samples prepared in a mixed solvent of glycerol and ethylene glycol with a ratio of 1:3. All samples are within the range of 15~80°, and have the same diffraction peaks at 16.34°, 26.83°, 31.59°, 38.32°, 47.41°, 50.46°, 55.33° and 58.07°, which are the same as the card (PDF-20-0782), corresponding to (111), (220), (311), (400), (422), (511), (440) and (620) crystal planes of $NiCo_2S_4$ (PDF-20-0782), respectively.[16, 17] Obviously, the longer the reaction time, the better the crystallinity of the corresponding sample. Therefore, the crystallinity of GENCS-1,3,6 samples is poor, while that of GENCS-9, 12, 15, 18 samples is obviously better than that of the previous. Certainly, the XRD also reflects that there is a fluctuation about crystallinity around 12 hours, which may be due to environmental factors. Figure 1(b) shows that the distribution of Ni, Co, and S in the detection tone is represented by an element mapping image, which further shows the coexistence of $NiCo_2S_4$.

3.2 Morphology characterization and Electrochemical characterization

Fig.2(a) and (b) are the SEM pictures of GENCS-1,3 and show that there are some opened cavities in the samples, which looks like a blooming flower. In fact, the TEM pictures, as shown in Fig.2(c), (d), present that the products are some irregular nano-particles with cavity. Our previous research suggests that when the cavity walls are thin, and at the same time the water pressure in the cavity is large enough, the cavity walls may be broke.[18, 19] Therefore, it can be inferred that the product is synthesized within 3 hour, and its cavity wall is thin,, and in this case the cavity wall is easily opened by a steam breakthrough. Fig.2(e), (f) show the lattice stripes and the spacing of the lattice stripes, which was measured to be 0.234nm, 0.186nm, 0.301nm and 0.297nm, respectively, corresponding to (400), (511), (220), (311) of $NiCo_2S_4$.

Some electrochemical measurements were also carried out here. It was tested their charge-discharge curve (GCD) and charge-discharge curve at different current densities. Fig.2(g), (h) show the GCD curves and rate curves, respectively. Using the GCD discharge curve of 1A/g current density, the discharge capacitance of the samples can be calculated to be 1874F/g and 1816F/g, respectively. But, at 10A/g, the calculated value is 1260F/g and 1620F/g, respectively. Obviously, GENCS-1 performance declined significantly with current rising, which may be related to its poor structural stability caused by its too thin cavity wall. Certainly, these two samples must benefit from their flower-like structure to achieve high capacitance performance. The open holes will expose more active sites, thereby increasing the ion exchange rate.

The SEM images of the remaining samples are shown in Fig.3(a) - (e). Their reaction time is 6h, 9h, 12h, 15h and 18h, respectively. It is observed that almost all these samples show platelet shapes, with a size of about 100 nm, but there is no any flower-like structure. This may indicate that when the reaction time is more than 6 hours, not only the cavity wall becomes thicker, but the atoms on the wall are arranged more orderly, which leads to stronger walls and all the cavities not to be broken again. The discharge test (GCD) and capacitance performance test under different current density conditions were performed on these samples, as shown in Fig. 3(f) and 3(g). These data indicate that at 1 A/g current density, the capacitance of these samples is between 1000~1600 F/g, and when the current density rises to 10 A/g, the capacitance attenuates between 960 and 1350 F/g, showing a significant slip compared to the previous two samples, especially compared with GENCS-3. It seems that the better the crystallinity, the worse the corresponding capacitance property. On the other hand, it can be seen from Fig. 2(h) and Fig.3 g that the rate performance of the samples with good crystallinity will be better. Therefore, GENCS-18 has a capacitance of 1020F/g at 1A/g and 960F/g at 10A/g, showing an excellent capacitance retention rate of 94.12%.

The CV curves of the GENCS-3 sample are also tested under different scanning rates of 5 mV/s, 10 mV/s, 20 mV/s, 30 mV/s, 40 mV/s, 50 mV/s and 100 mV/s, as shown in the Fig. 5(a). It can be seen in the figure that with the increase of scanning rate, the area of the curve also increases, and the position of the redox peak also moves to both ends. Due to the change of sweep speed, the polarization of the electrode occurs, and the redox peak current is also increasing. In a certain voltage range, the peak current does not reach the peak point, so the peak is moving. Fig. 5(b) shows the GCD curves of the GENCS-3 at 1 A/g, 3 A/g, 5 A/g, 8 A/g and 10 A/g in a potential window of 0-0.5. It can be seen that all GCD curves have symmetry under different current density, indicating that the sample has good charge-discharge reversibility. Based on Fig. 5(b), the specific capacitance of GENCS-3 is calculated under different current density, showing a value of 1816 F/g, 1752F/g, 1710F/g, 1648F/g, 1620F/g, respectively. Fig. 5(c) provides the CV curves of all samples at 5 mV/s sweep speed, and there are obvious redox peaks of pseudocapacitance, which are mainly attributed to the Faraday redox reaction between Co^{2+}/Co^{3+} (Ni^{2+}/Ni^{3+}) cations and OH^- anions. Fig. 5(d), (e) shows the impedance plots of the low-frequency and high-frequency regions of all the samples, respectively, where the intercept of the curve with the X axis represents the base resistance of the electrode solution. It can be seen from the figure that the slope of

GENCS-3 in the low frequency region is greater than that of other samples. This shows that its ion transmission efficiency to electrolyte is better than others. The EIS of GENCS-1, 3 has a larger slope in the low frequency region, indicating their better diffusion behavior.[20] However, the Rs value (4.4 Ω) of the sample GENCS-1 is much greater than that of the sample GENCS-3 (0.5 Ω).

Fig. 5(f) shows the $Ip \sim v^{1/2}$ fitting curve of the oxidation peak of the cyclic voltammetry curve of all samples at different scan rates. Here, Ip is the peak electricity (A) of the oxidation peak or reduction peak and v is the cycle Scanning rate of ring voltammetry (mV/s). The oxidation peak current (Ip) is proportional to the square root of the scan rate, indicating that the process of OH^- embedding in the $NiCo_2S_4$ electrode is a diffusion process. The relationship between CV peak current (Ip) and scan rate is:

$$D_{OH^-} \propto \frac{Ip}{v^{1/2}} \qquad (1)$$

Where is the OH^- diffusion coefficient. The fitting curve slope of sample GENCS-3 is 1.5, which is much larger than that of other sample fitting curves. Therefore, the diffusion coefficient () of GENCS-3 sample is larger than that of other samples, thus showing excellent electrochemical performance. Fig. 5(g) is retention rate chart of all samples. It can be seen that the retention rate of GENCS-3 is 89.5%, which is a little lower than that of the GENES-18, not to exceed 5%. The degradation is due to the long-term cycling that causes certain damage to the electrode.

Here are two samples selected for BET testing, one with maximum capacitance and the other with minimum capacitance. Fig. 6(a), (b) show that the BET results of the samples of GENCS-3 and GENCS-18, respectively. As showing in Fig. 6(a), (b), both samples have many micropores, few mesopores, and few macrospores. However, the pore size of GENCS-3 is mostly in the micropore area, while the pore size distribution of GENCS-18 is not very uniform in the pore area, and the pore size fluctuates greatly. The average pore size of GENCS-3 is 7nm, and that of GENCS-18 is 10nm. And GENCS-3 has the surface area of 40.3953 m^2/g, but the GENCS-18 only has a surface area of 10.2466 m^2/g. As thought, GENCS-3 has a larger specific surface area, which is mainly due to its poor crystallinity and more defects. Of course, larger specific surface area can enlarge the effective release area between the electrode and the electrolyte ions, which is beneficial to enhance the diffusion of electrolyte ions in the electrode, thereby improving electrochemical performance.[21]

4. Conclusions

In this paper, the double solvothermal method is used to prepare nickel cobalt sulfide nanoparticles with closed cavity in irregular shape. The synthesis time was selected to control the crystallinity. It is found that for samples with synthesis time less than 3 hours, the crystallinity is poor, but there are some open cavities in the body, like flowers, which is beneficial to increase the capacitance. As the synthesis time is

more than 6 hours, the longer the time, the better the crystallinity of the obtained sample, and the corresponding rate performance will be better. The best sample is GENCS-3 with a short reaction time of 3hour, which has flower-like structures, and also has good ion transmission efficiency excellent specific capacitance (1816F/g at 1A/g, 1620F/g at 10 A/g) and good retention rate of 89.5%. Our study shows that nickel-cobalt sulfide with weak crystallinity is easy to form porous structure, which can significantly increase capacitance, but may lose a little rate performance. Of course, the loss is controllable and does not exceed 5 per cent

Declarations

This research was financially supported by the National Natural Science Foundation of China (No. 52020105011).

References

1. Gao, M.; Wang, W. K.; Rong, Q.; Jiang, J.; Zhang, Y. J.; Yu, H. Q., Porous ZnO-Coated Co3O4 Nanorod as a High-Energy-Density Supercapacitor Material. ACS Appl Mater Interfaces 2018, 10 (27), 23163-23173.
2. Wang, R.; Luo, Y.; Chen, Z.; Zhang, M.; Wang, T., The effect of loading density of nickel-cobalt sulfide arrays on their cyclic stability and rate performance for supercapacitors. Science China Materials 2016, 59 (8), 629-638.
3. Qirui; Liang; Huihui; Jin; Zhe; Wang; Yuli; Xiong; Energy, S. J. N., Metal-organic frameworks derived reverse-encapsulation Co-NC@Mo2C complex for efficient overall water splitting. 2019.
4. Candelaria, S. L.; Uchaker, E.; Cao, G., Comparison of surface and bulk nitrogen modification in highly porous carbon for enhanced supercapacitors. Science China Materials 2015, 58 (7), 521-533.
5. Liu, Y.; Huang, B.; Lin, X.; Xie, Z., Correction: Biomass-derived hierarchical porous carbons: boosting the energy density of supercapacitors via an ionothermal approach. Journal of Materials Chemistry A 2017, 5 (47), 25090-25090.
6. Science News, S., Researchers welcome Trump's pick to head science office. Science 2018, 361 (6401), 434.
7. Wu, Z.-S.; Feng, X.; Cheng, H.-M., Recent advances in graphene-based planar micro-supercapacitors for on-chip energy storage. National Science Review 2014, 1 (2), 277-292.
8. In situ synthesis of MoS2/graphene nanosheets as free-standing and flexible electrode paper for high-efficiency hydrogen evolution reaction %J Rsc Advances. 2018, 8 (19), 10698-10705.
9. Xiao, J.; Yang, S., Sequential crystallization of sea urchin-like bimetallic (Ni, Co) carbonate hydroxide and its morphology conserved conversion to porous NiCo2O4 spinel for pseudocapacitors. RSC Advances 2011, 1 (4).
10. Zhang, S.; Zhu, Y.; Kong, C.; Shi, C.; Tao, X.; Zhang, D., Adjustment of Nickel Cobalt Sulfide morphology with double solvents for its excellent charge-discharge performance. Materials Science

in Semiconductor Processing 2019, 93, 99-104.

11. Zhang, Y.; Ma, M.; Yang, J.; Sun, C.; Su, H.; Huang, W.; Dong, X., Shape-controlled synthesis of NiCo2S4 and their charge storage characteristics in supercapacitors. Nanoscale 2014, 6 (16), 9824-30.
12. Zhang, S.; Zhu, Y.; Tang, X.; Shi, C.; Gu, X.; Zhang, D. J. J. o. M. S. M. i. E., Sulfidation of cobalt nickel oxide nanofibers for improving their specific capacity. 2018, 29 (24), 20800-20807.
13. Zhang, S.; Zhu, Y.; Kong, C.; Shi, C.; Tao, X.; Zhang, D. J. M. S. i. S. P., Adjustment of Nickel Cobalt Sulfide morphology with double solvents for its excellent charge-discharge performance. 2019, 93, 99-104.
14. Zhang, S.; Zhu, Y.; Kong, C.; Shi, C.; Liu, W. J. J. o. M. e. M. i. E., The different electrochemical performance of nickel–cobalt sulfide and its formation mechanism of honeycomb-like structure. 2019, 30 (17).
15. Zhang, S.; Huang, B. S.; Shi, C.; Xu, Q.; Zhu, Y. J. C.; Physicochemical, S. A.; Aspects, E., Design of electrode Materials of Nickel-Cobalt compounds for aqueous Symmetrical supercapacitor with Large Power and High Energy Density. 2020, 125243.
16. Xiao, Y.; Lei, Y.; Zheng, B.; Gu, L.; Wang, Y.; Xiao, D., Rapid microwave-assisted fabrication of 3D cauliflower-like NiCo2S4 architectures for asymmetric supercapacitors. RSC Advances 2015, 5 (28), 21604-21613.
17. Zhang, Z.; Wang, X.; Cui, G.; Zhang, A.; Zhou, X.; Xu, H.; Gu, L., NiCo2S4 sub-micron spheres: an efficient non-precious metal bifunctional electrocatalyst. Nanoscale 2014, 6 (7), 3540-4.
18. Lei, J.; Zhu, Y.; Chen, Z.; Liu, W.; Zhang, D., Improving the electrochemical performance of Nano-PANI by adding manganese. Journal of Materials Science: Materials in Electronics 2018, 29 (14), 12366-12372.
19. Zhang, S.; Zhu, Y.; Kong, C.; Shi, C.; Xu, Q.; Liu, W., The different electrochemical performance of nickel–cobalt sulfide and its formation mechanism of honeycomb-like structure. Journal of Materials Science: Materials in Electronics 2019, 30 (17), 16000-16007.
20. Gao, M.; Wang, W.-K.; Zhang, X.; Jiang, J.; Yu, H.-Q., Fabrication of Metallic Nickel–Cobalt Phosphide Hollow Microspheres for High-Rate Supercapacitors. The Journal of Physical Chemistry C 2018, 122 (44), 25174-25182.
21. Elkin, V. V.; Krotova, M. D.; Pleskov, Y. V., Polarization complex-plane plot of impedance for two-stage charge-transfer reaction complicated with an intermediate adsorption (by example of benzene oxidation at boron-doped diamond electrode). Electrochimica Acta 2014, 144, 412-418.

Figures

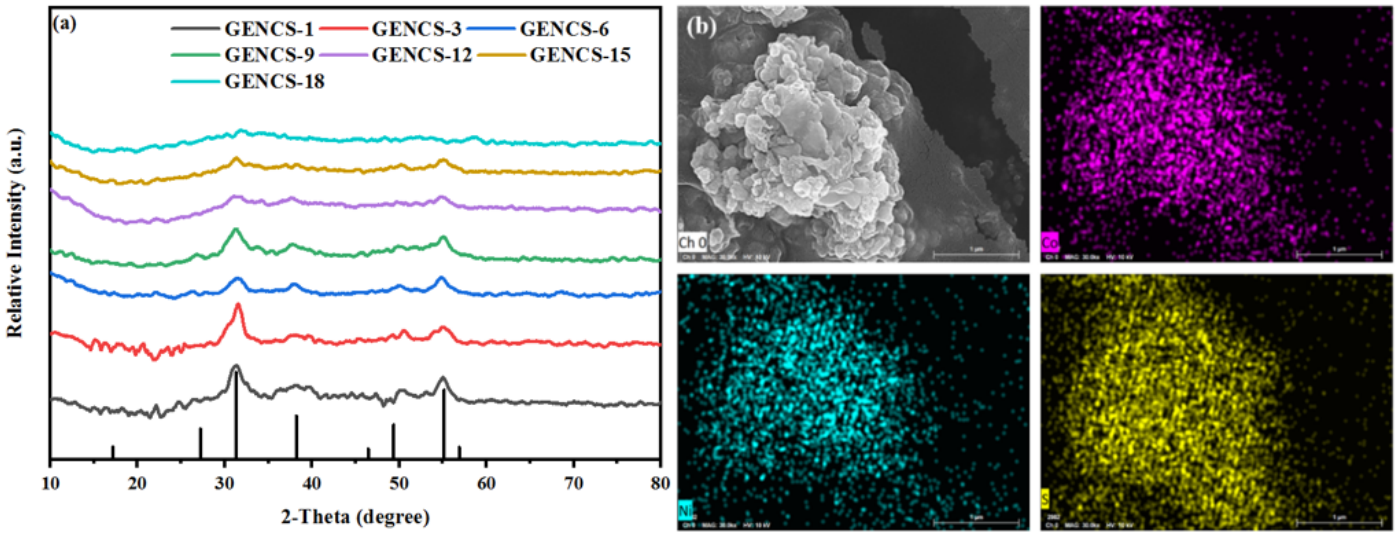

Figure 1

(a) XRD patterns and (b) EDS element mapping of GENCS-3 sample

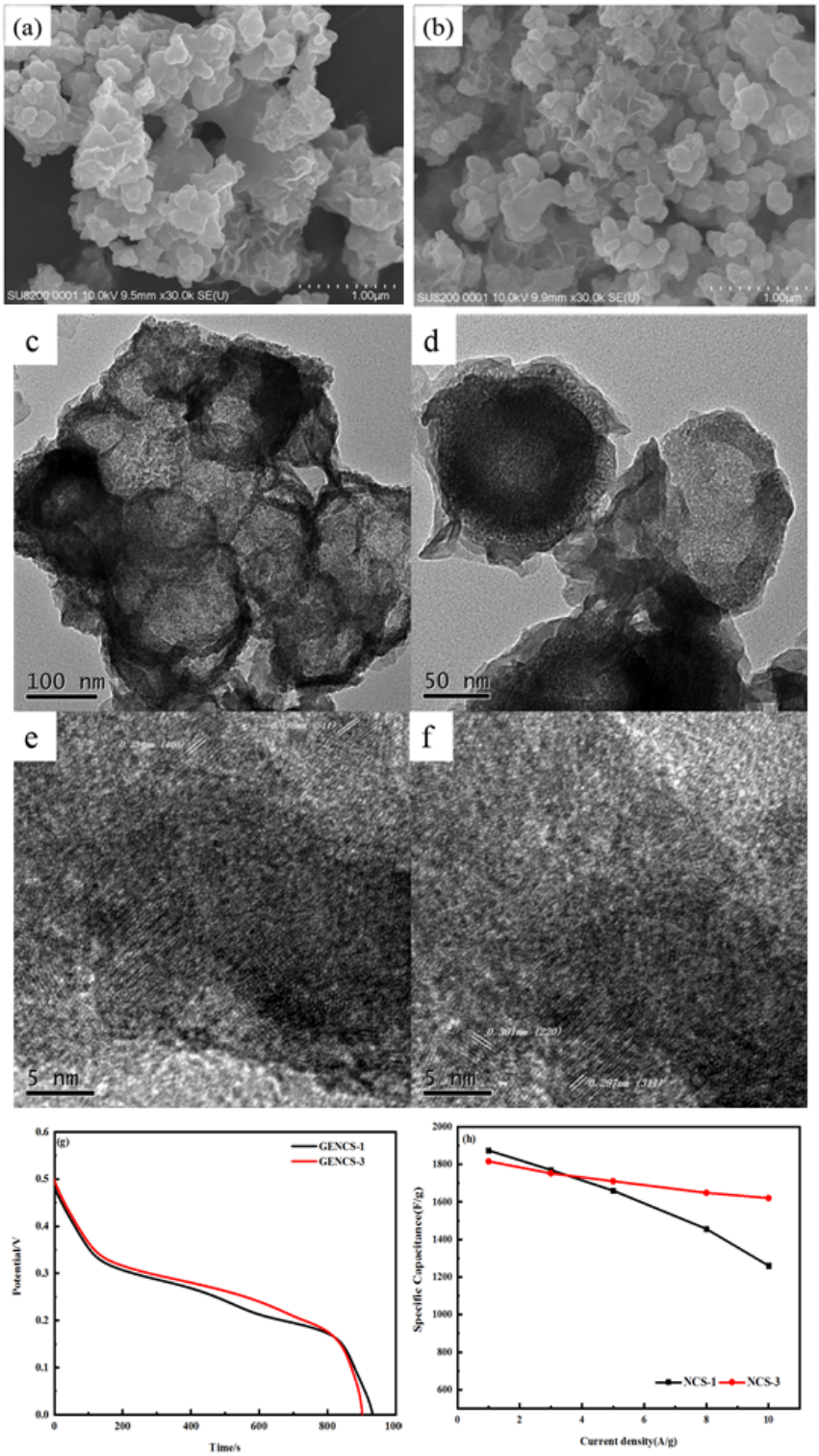

Figure 2

SEM of GENCS-1 (a), GENCS-3 (b), TEM image and HRTEM image of GENCS-3 (c, d, e, f), GCD graph of them (g) at current density of 1A/g and their capacitance curve diagram under different current density conditions (h)

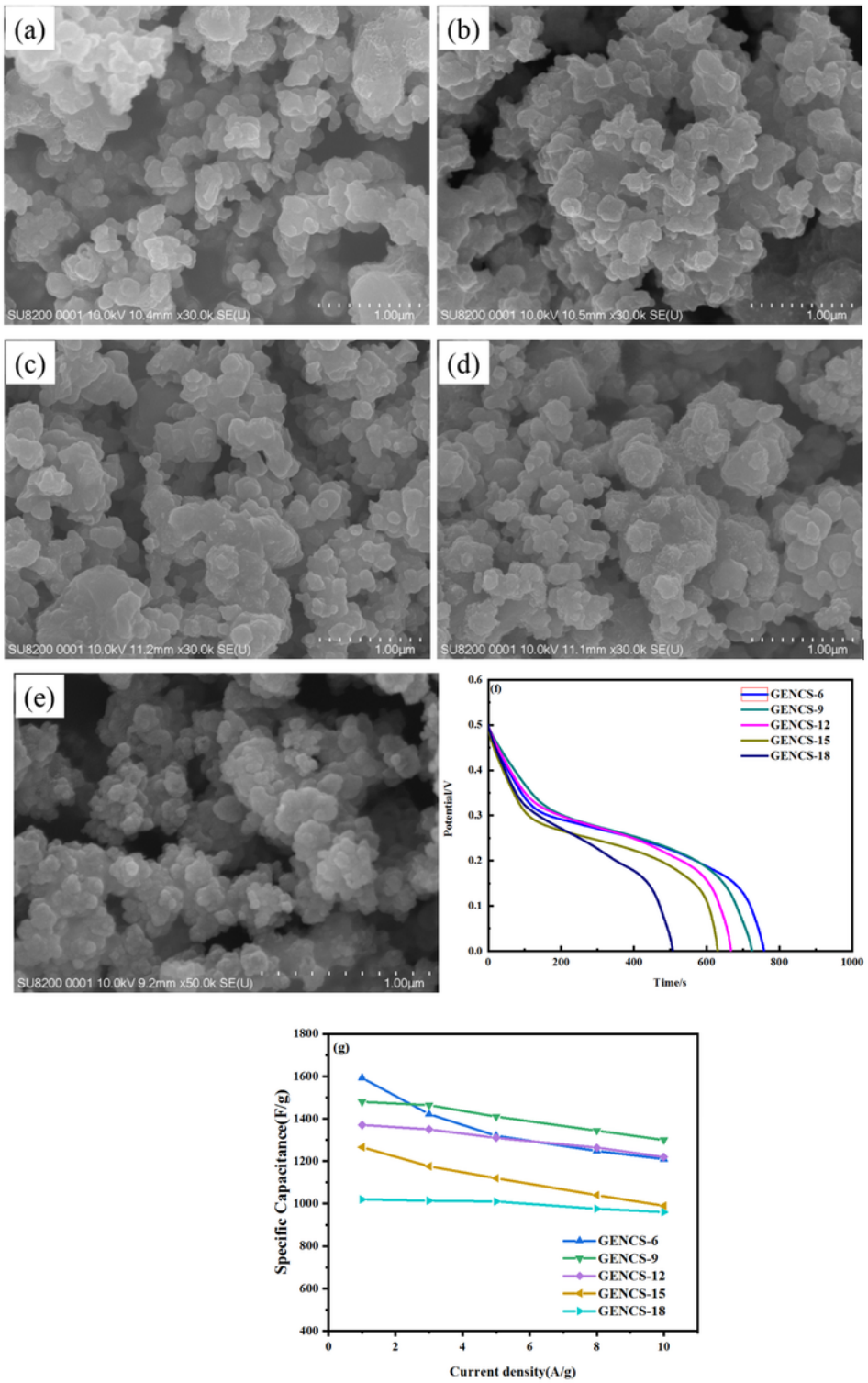

Figure 3

SEM of GENCS-6 (a), GENCS-9 (b), GENCS-12 (c), GENCS-15 (d), GENCS-18 (e) , GCD curve of these samples at current density of 1A/g (f) and their capacitance curve diagram under different current density (g)

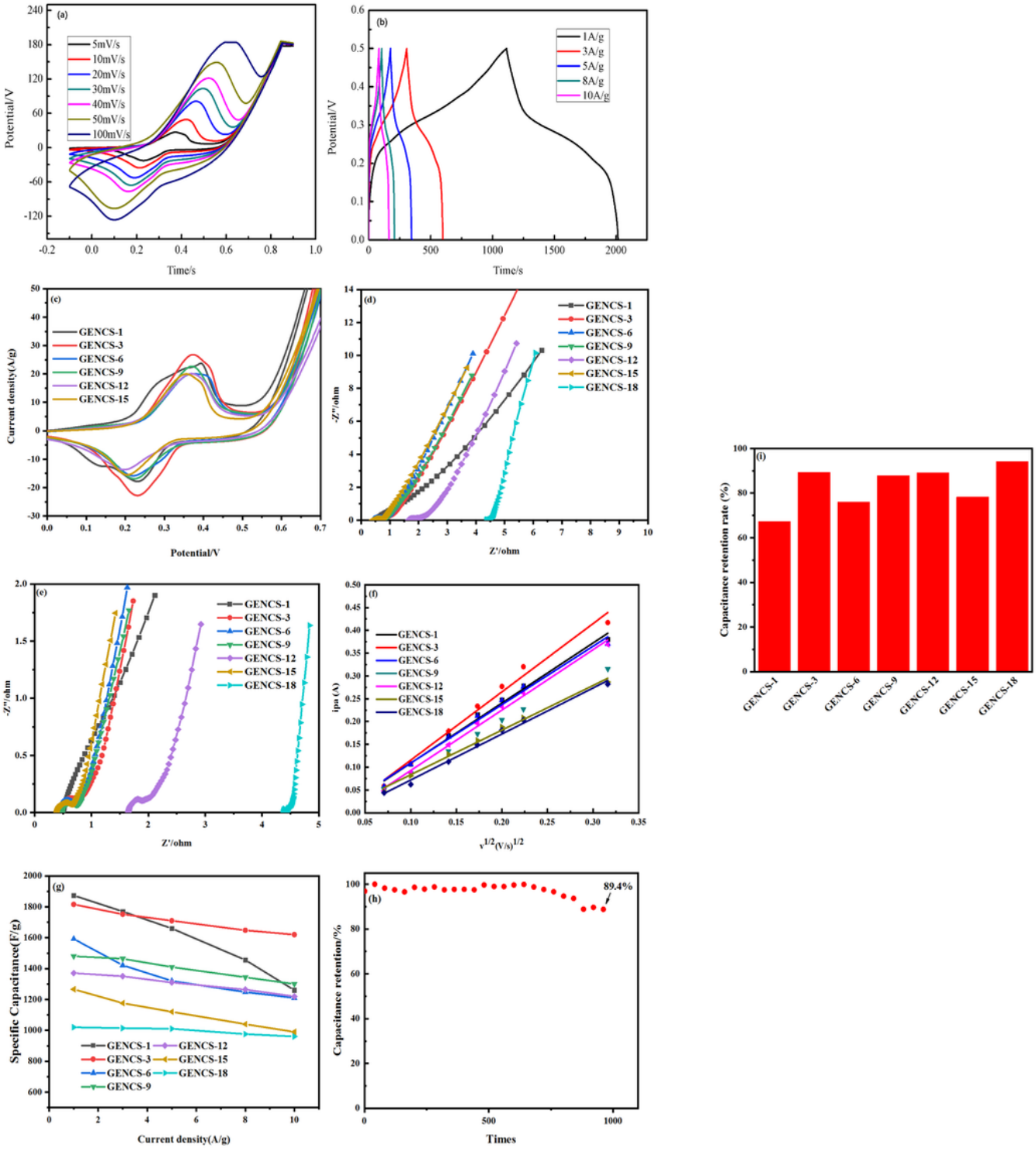

Figure 4

(a) CV and (b) GCD plots of GENCS-3, (c) CV plots of all samples at 5 mV/s, (d), (e) Graphs EIS low-frequency and high-frequency regions for all samples, (f) the peak current (Ip) of all samples as a function of scan rate (v), (g) specific capacitance and current density of all samples, (h) cyclic stability of GENCS-3 at 5A/g and (i) Rate chart of all samples

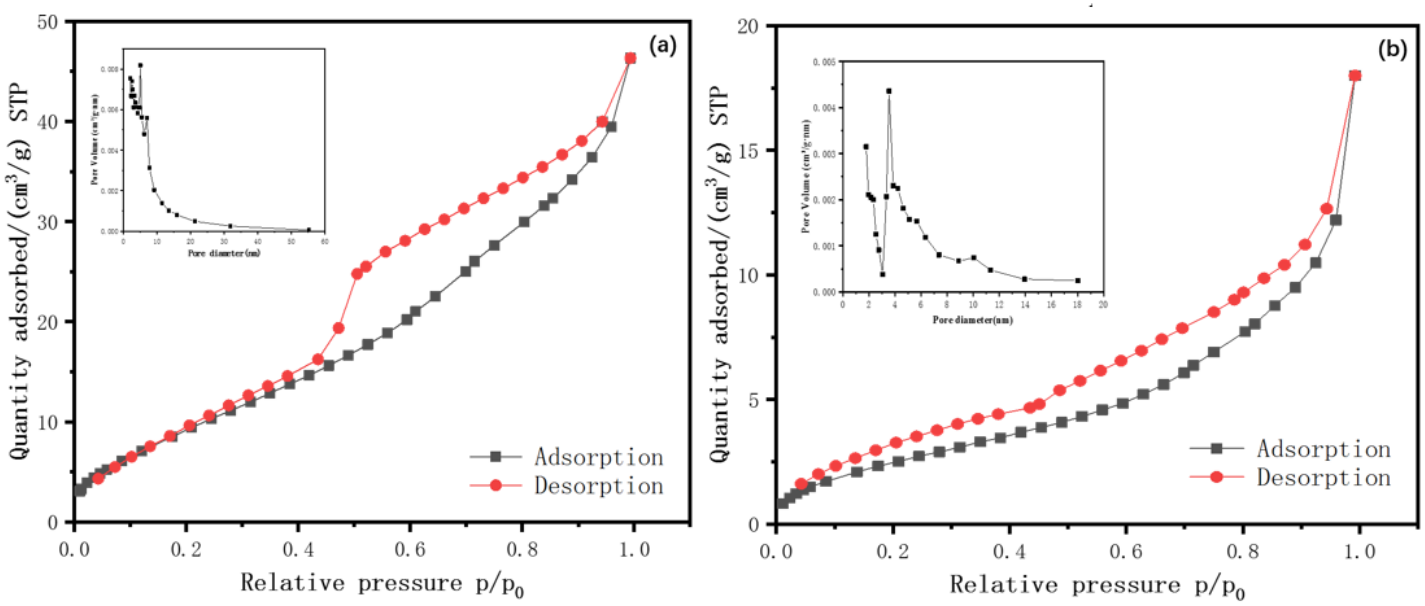

Figure 5

The nitrogen adsorption and desorption isotherms of GENCS-3 (a), GENCS-18 (b), respectively. The corresponding pore size distribution is inlaid in the figure.